Research Article

Yogesh Dadhich, Reema Jain*, Karuppusamy Loganathan*, Mohamed Abbas, Kalyana Srinivasan Prabu, and Mohammed S. Alqahtani

Sisko nanofluid flow through exponential stretching sheet with swimming of motile gyrotactic microorganisms: An application to nanoengineering

https://doi.org/10.1515/phys-2023-0132
received July 19, 2023; accepted October 13, 2023

Abstract: The swimming of motile gyrotactic microorganism's phenomenon has recently become one of the most important topics in research due to its applicability in biotechnology, many biological systems, and numerous engineering fields. The gyrotactic microorganisms improve the stability of the nanofluids and enhance the mass/heat transmission. This research investigates the MHD fluid flow of a dissipative Sisko nanofluid containing microorganisms moving along an exponentially stretched sheet in the current framework. The mathematical model comprises equations that encompass the preservation of mass, momentum, energy, nanoparticle concentration, and microorganisms. The equations that govern are more complicated because of nonlinearity, and therefore to obtain the combination of ordinary differential equations, similarity transformations are utilized. The numerical results for the converted mathematical model are carried out with the help of the bvp4c solver. The resulting findings are compared to other studies that have already been published, and a high level of precision is found. The graphical explanations for velocity, temperature, and nanoparticles volume fraction distribution are shown with physical importance. Physical characteristics like Peclet number, Sisko fluid parameter, thermophoresis and Brownian motion parameter, and Hartmann number are taken into consideration for their effects. Based on the numerical outcomes, the bioconvection Peclet number enhances the density of mobile microorganisms, whereas thermal radiation contributes to an elevation in temperature. The velocity field decreases with the enhancement of magnetic parameter; however, the temperature field increases with increased magnetic parameter and thermophoresis parameter augmentation. Our numerical findings are ground breaking and distinctive, and they are used in microfluidic devices including micro instruments, sleeve electrodes, and nerve development electrodes. This study has various applications in nanoengineering, including nanomaterial synthesis, drug delivery systems, bioengineering, nanoscale heat transfer, environmental engineering.

Keywords: MHD, nanofluid, Sisko model, microorganisms, exponentially stretched sheet

*** Corresponding author: Reema Jain,** Department of Mathematics and Statistics, Manipal University Jaipur, Jaipur 303007, Rajasthan, India, e-mail: reemajain197@gmail.com
*** Corresponding author: Karuppusamy Loganathan,** Department of Mathematics and Statistics, Manipal University Jaipur, Jaipur 303007, Rajasthan, India, e-mail: loganathankaruppusamy304@gmail.com
Yogesh Dadhich: Department of Mathematics and Statistics, Manipal University Jaipur, Jaipur 303007, Rajasthan, India
Mohamed Abbas: Electrical Engineering Department, College of Engineering, King Khalid University, Abha 61421, Saudi Arabia, e-mail: mabas@kku.edu.sa
Kalyana Srinivasan Prabu: Department of Physics, Kongu Engineering College, Erode, Tamil Nadu, India, e-mail: kprabhu.sh@kongu.edu
Mohammed S. Alqahtani: Radiological Sciences Department, College of Applied Medical Sciences, King Khalid University, Abha 61421, Saudi Arabia; BioImaging Unit, Space Research Centre, Michael Atiyah Building, University of Leicester, Leicester, LE1 7RH, United Kingdom, e-mail: mosalqhtani@kku.edu.sa

Nomenclature

A	material parameter (–)
B_0	magnetic field strength (kg s^{-2} A^{-1})
C	concentration (kg m^{-3})
C_∞	ambient concentration (kg m^{-3})
C_w	sheet concentration (kg m^{-3})
c_p	specific heat (J kg^{-1} K^{-1})
d	chemotoxis constant (m)
D_B	coefficient of Brownian diffusion (m^2 s^{-1})

D_m	microorganism diffusion coefficient ($m^2\ s^{-1}$)
D_T	coefficient of thermophoretic diffusion ($m^2\ s^{-1}$)
E_c	Eckert number (−)
k	thermal conductivity ($W\ m^{-1}\ K^{-1}$)
L_b	bioconvection Lewis number (−)
L_e	Lewis parameter (−)
M	magnetic field parameter
N_b	Brownian diffusion parameter
N_t	thermophoresis parameter
Nu_x	local Nusselt number
N	concentration of microorganisms ($kg\ m^{-3}$)
N_w	sheet concentration of microorganisms ($kg\ m^{-3}$)
N_∞	ambient concentration of microorganisms ($kg\ m^{-3}$)
P_e	Peclet number
P_r	Prandtl number
q_r	radiative heat flux ($W\ m^{-2}$)
R	radiation parameter
Re_a,Re_b	local Reynolds numbers
Sh_x	Sherwood number
T	fluid temperature (K)
T_w	sheet temperature (K)
T_∞	ambient fluid temperature (K)
u,v	velocity components ($m\ s^{-1}$)
W_c	maximum cell swimming speed ($m\ s^{-1}$)
x,y	Cartesian coordinates (m)

Greek symbols

α	thermal diffusivity ($m^2\ s^{-1}$)
δ	heat source/sink parameter
η	similarity parameter
θ	temperature similarity function
ϕ	concentration similarity function
χ	microorganism similarity function
λ	mixed convection parameter
ϑ	kinematic viscosity ($m^2\ s^{-1}$)
ρ	density ($kg\ m^{-1}$)
τ	ratio of the effective heat capacity
σ	electrical conductivity (S/m)

Subscripts

∞	ambient condition
w	surface condition

1 Introduction

Numerous biological, industrial, and technical processes, such as the production of fibres, refinement of polymer, hot roll glass blasting, heat exchangers, extrusion of aerodynamics, MHD power generators, domestic refrigerator-freezers, rubber and plastic sheet manufacturing, cooling process of reactors, improving diesel generator efficiency, and cooling/drying of papers, the flow of nanofluid over stretching or shrinking sheets is extremely important [1]. Nanofluids may be useful in solar energy, nuclear reactors, medicine delivery, and cancer treatment. Nanoparticle scattering in common (base) fluids yields nanofluids. Polymer solutions can be utilized as base fluids in addition to normal fluids including oils and lubricants. Choi *et al.* [2] were the first to present the fundamental concept of such metallic nanoparticles by presenting a comprehensive model for improving the thermal characteristics of base fluid. Subsequently, Buongiorno [3] established a non-homogeneous equilibrium model by incorporating Brownian movement and thermophoresis properties to describe the slip mechanism of nanoparticles. Eastman *et al.* [4] explored the phenomena of heat transfer in the presence of copper oxide (CuO) particles made of water and Al_2O_3 particles made of ethylene glycol. Since then, Sheikholeslami *et al.* [5] have explored the properties of nanofluids. Pourfattah *et al.* [6] employed two-phase flow simulation to investigate the characteristics of microchannel heat sink. The processing methods and thermal characteristics of oil-based nanofluid were investigated by Asadi *et al.* [7]. Khan *et al.* [8] investigated the fluid flow of nanoparticles for the Jeffrey fluid. An experimental study on the effects of ultra-sonication of MWCNT-H_2O nanofluid was carried out by Asadi *et al.* [9]. Zeeshan *et al.* [10] conducted an analysis on the movement of two immiscible fluids within a lengthy, flexible tube. They formulated models for both the core and peripheral regions, making assumptions of long wavelength behaviour and creeping flow. Riaz *et al.* [11] explored the transportation of nanosized particles through a curved channel characterized by non-Darcy porous conditions. The flow in this channel is driven by a peristaltic wave. Riaz *et al.* [12] analyzed the effects of an applied magnetic field and entropy generation on Jeffrey nanofluid in the annular section between two micro non-concentric pipelines, with the inner pipe being rigid and moving at a constant speed. The researchers discovered that the magnetic field reduced the flow velocity and the rate of entropy production while increasing the temperature of the nanofluid. Following that, other researchers and technologists worked in the same field, and numerous publications have been published that

consider the existence of nanofluids and magnetic fields in addition to linear and nonlinear thermal radiation, chemical reactions, and other factors [13–15].

Bioconvection occurs when bacteria spread randomly in a single-celled and, in certain cases, colony-like pattern. Because of the gyrotactic microorganisms upstream, the buoyancy of the fluid significantly increases. The flow of microbes in nanofluids has recently drawn the attention of researchers due to wide applications in biosensors, microbial-enhanced oil recovery, engineering, biological, and chemical fields such as biofuels, cancer treatment, enzymes, biotechnological applications, production and manufacturing, industrial level, and others. Firstly, Kuznetsov [16] established the concept of nanofluid bioconvection. Later, using Navier–Stokes equations, Alloui *et al.* [17] examined the distribution of microorganisms in a cylinder. Waqas *et al.* [18] used the magnetic dipole effect to investigate the bioconvection effect that microbes produce in Jeffery nanofluid through an expanded surface. Waqas *et al.* [19] presented a computational investigation of nanofluid flow (Oldroyd-B Model) with mass and heat transport, gyrotactic microbes past a rotating disc using the MATLAB built-in function bvp4c. Uddin *et al.* [20] first described the blowing effect on bio-convection flow across a dynamic stretched sheet. Following that, Chamkha *et al.* [21] described the bioconvective fluid flow containing microbes through a radiating stretching plate. Using the help of a nanofluid model of Buongiorno's and the O.-Boussinesq approximation, Rashad and Nabwey [22] examined the bio-convection flow containing microorganisms through a cylinder placed horizontally under convective boundaries. Alwatban *et al.* [23] investigated bioconvection using slip effects of Wu's at the surface. Aziz *et al.* [24] anticipated a bioconvective flow of microorganisms embedded in the porous medium. Shaw *et al.* [25] used a spectrum relaxation technique to derive the associated equations depicting the fluid nanoflow with microorganisms. Rashad and Nabwey [22] and Rashad *et al.* [26] recently addressed the subject of bioconvection over a vertical thin cylinder. Elboughdiri *et al.* [27] investigated radiating viscoelastic nanofluids in MHD mixed convective flows near a sucked impermeable surface with exponentially decreasing heat generation using Jeffery's model, convective mass transport, thermophoresis, and Brownian diffusion under boundary layer assumptions. The influence of nanoparticles on the thermosolutal sensitivity of non-Newtonian fluid flow is investigated by Sharma *et al.* [28], with numerical computations employing blood as the base liquid. Wakif [29] computed the two-dimensional mixed convective motion of a radiating mixture of an upper-convected Maxwell nanofluid and gyrotactic motile microorganisms along a convectively heated vertical surface with a uniform magnetic field source, revealing the non-homogeneous appearance and dynamical properties of the system. Puneeth *et al.* [30] investigation focuses on analysing the impact of Brownian motion and thermophoresis on the flow of a tangent hyperbolic (pseudoplastic) nanofluid past a rotating cone in three-dimensional free stream conditions.

Observations from previous studies reveal the lack of evidence regarding the flow of dissipative magneto Sisko-nanofluid with gyrotactic microorganisms along an exponentially stretching sheet. The goal of this study is to describe the heat transfer properties of bioconvection flow of Sisko nanofluid along an exponential stretched sheet. To obtain a simplified mathematical model, similarity transformations are employed. The computational analysis is completed using the bvp4c and coding MATLAB scripts. Graphical analysis is used to explore the behaviour of the relevant parameters, and results are compared with the earlier research. For designing equipment, such as electric ovens, electric heaters, microelectronics, and wind generators, the thermal industry uses these kinds of modelled problems. The study aims to analyse the behaviour of the nanofluid flow and the influence of the motile microorganisms, with potential applications in the field of nanoengineering.

2 Mathematical modelling

2.1 Rheological model

Consider a non-Newtonian fluid that is time independent and follows the Sisko rheological model; the Cauchy stress tensor for such fluids is defined as follows:

$$\mathbf{T} = -p\mathbf{I} + \mathbf{S},$$

where $\mathbf{S}$ is the extra stress tensor and is expressed as follows:

$$\boldsymbol{S} = \left[\boldsymbol{a} + \boldsymbol{b}\left|\sqrt{\frac{1}{2}\mathbf{tr}(\boldsymbol{A}_1^2)}\right|^{n-1}\right]\boldsymbol{A}_1,$$

where for "$n > 0$ for various fluids," a and b are the physical constants difference, $\boldsymbol{A}_1 = (\text{grad } V) + (\text{grad } V)^{\mathrm{T}}$, V represents for the vector as velocity, and T stands for transposition and means the first Rivlin–Erickson tensor.

2.2 Governing equations and boundary conditions

The flow configuration of the current investigation is illustrated in Figure 1, which shows the movement of a two-dimensional laminar boundary layer dissipative Sisko

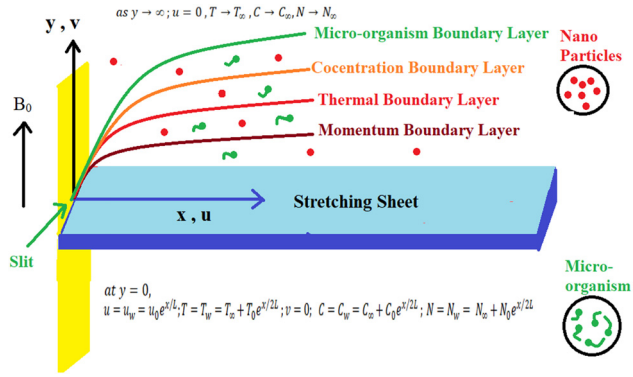

Figure 1: Physical model.

nanofluid containing microbes across an exponentially stretched surface, under steady conditions (independent of time). Here, the sheet was stretched exponentially along the x-axis with a stretching velocity $u_w(x) = u_0 e^{x/L}$ to initiate the flow of nanofluids. The effects of viscous dissipation, magnetic field, and Brownian motion are addressed in flow formulation. The x and y-axes are assumed perpendicular to each other. A fixed magnetic field, B_0, is acted parallel to the y-direction upon. u and v represent the velocity components along the x and y axes, respectively. Furthermore, the assumption is made that the temperature, nanoparticle volume fraction, and density of motile microbes on the stretchable surface are T_w, C_w, and N_w, respectively. In addition, it is considered that these variables remain constant as T_∞, C_∞, and N_∞ when moving away from the stretchable surface.

Using the assumptions stated earlier, the fundamental equations for the present investigation can be addressed as follows [31]:

Continuity equation:

$$\frac{\partial u}{\partial x} + \frac{\partial v}{\partial y} = 0. \tag{1}$$

Momentum equation:

$$u\frac{\partial u}{\partial x} + v\frac{\partial u}{\partial y} = \frac{a}{\rho}\frac{\partial^2 u}{\partial y^2} - \frac{b}{\rho}\frac{\partial}{\partial y}\left(-\frac{\partial u}{\partial y}\right)^n - \frac{\sigma B_0^2 u}{\rho}. \tag{2}$$

Thermal energy equation:

$$\begin{aligned} u\frac{\partial T}{\partial x} + v\frac{\partial T}{\partial y} = {} & \alpha\frac{\partial^2 T}{\partial y^2} + \tau\left[D_B\frac{\partial C}{\partial y}\frac{\partial T}{\partial y} + \frac{D_T}{T_\infty}\left(\frac{\partial T}{\partial y}\right)^2\right] \\ & - \frac{1}{(\rho C_p)_f}\frac{\partial q_r}{\partial y} + \frac{Q}{(\rho C_p)_f}(T - T_\infty) \\ & + \frac{1}{(\rho C_p)_f}\left[a\left(\frac{\partial u}{\partial y}\right)^2 + b\left(-\frac{\partial u}{\partial y}\right)^{n+1}\right] \\ & + \frac{\sigma B_0{}^2 u^2}{(\rho C_p)_f}. \end{aligned} \tag{3}$$

Nanoparticle concentration equation:

$$u\frac{\partial C}{\partial x} + v\frac{\partial C}{\partial y} = D_B\frac{\partial^2 C}{\partial y^2} + \frac{D_T}{T_\infty}\frac{\partial^2 T}{\partial y^2}. \tag{4}$$

Conservation equation for microorganisms:

$$u\frac{\partial N}{\partial x} + v\frac{\partial N}{\partial y} - D_m\frac{\partial^2 N}{\partial y^2} + \frac{dW_c}{C_w - C_\infty}\left[\frac{\partial}{\partial y}\left(N\frac{\partial C}{\partial y}\right)\right] = 0. \tag{5}$$

The corresponding boundary conditions are as follows:

$$\begin{aligned} &\text{at } y = 0 : u = u_w = u_0 e^{x/L};\ v = 0;\ T = T_w; \\ &C = C_w;\ N = N_w, \end{aligned} \tag{6}$$

$$\text{at } y \to \infty;\ u = 0,\ T \to T_\infty,\ C \to C_\infty,\ N \to N_\infty. \tag{7}$$

The following transformations are used to convert the aforementioned equations into their non-dimensional forms [32]:

$$\begin{aligned} \eta &= y\sqrt{\frac{u_0}{2\vartheta L}}\,e^{x/2L} \\ u &= u_0 e^{x/L} f'(\eta) \\ v &= -\sqrt{\frac{u_0\vartheta}{2L}}\,e^{x/2L}[f(\eta) + \eta f'(\eta)] \\ \theta(\eta) &= \frac{T - T_\infty}{T_w - T_\infty} \\ \phi(\eta) &= \frac{C - C_\infty}{C_w - C_\infty} \\ \chi(\eta) &= \frac{N - N_\infty}{N_w - N_\infty}. \end{aligned} \tag{8}$$

The radiative heat flux q_r is determined using the Rosseland diffusion approximation and is given by

$$q_r = -\frac{4\sigma^*}{3k^*}\frac{\partial T^4}{\partial y}. \tag{9}$$

The Rosseland mean absorption coefficient is denoted as k^*, and the Stefan–Boltzmann constant is represented by σ^*. Assuming minimal temperature variations within the flow, T^4 can be expressed as a linear function of temperature.

$$T^4 = 4T_\infty^3 - 3T_\infty^4. \tag{10}$$

Using Eqs. (9) and (10)

$$\frac{\partial q_r}{\partial y} = -\frac{16\sigma^* T_\infty^3}{3k^*}\frac{\partial^2 T}{\partial y^2}, \tag{11}$$

where η shows similarity parameter; $f(\eta)$ indicates dimensionless stream function; $\theta(\eta)$ represents dimensionless temperature; and $f'(\eta)$ shows the dimensionless velocity profile (the derivative of $f(\eta)$).

By utilizing the non-dimensional similarity parameters given below, Eqs. (1)–(7) can be converted into

dimensionless equations. The given equations are converted into their non-dimensional forms using the following transformations:

$$Af''' + n(-f'')^{n-1}f''' - Mf' - 2f'^2 + ff'' = 0, \tag{12}$$

$$\left(1 + \frac{4R}{3}\right)\theta'' + P_r f\theta' + \delta P_r\theta + N_b\theta'\phi' + N_t\theta'^2 + MP_rE_cf'^2 + AP_rE_c(f'')^2 + P_rE_c(-f'')^{n+1} = 0, \tag{13}$$

$$\phi'' + P_rL_e f\phi' + \left(\frac{N_t}{N_b}\right)\theta'' = 0, \tag{14}$$

$$\chi'' + L_b f\chi' - [P_e(\phi''\chi + \phi'\chi')] = 0. \tag{15}$$

Furthermore, the boundary conditions are modified as follows: at

$$\eta = 0 \ : \ f'(\eta) = 1; f(\eta) = 0; \theta(\eta) = 1; \phi(\eta) = 1; \chi(\eta) = 1, \tag{16}$$

for

$$\eta \to \infty \ : \ f'(\eta) = 0; \theta(\eta) = 0; \phi(\eta) = 0; \chi(\eta) = 0. \tag{17}$$

In Eqs. (12)–(17), the prime indicates the differentiation with respect to η (similarity parameter). The following non-dimensionless parameters are used:

$$L_b = \frac{\alpha}{D_m}; P_e = \frac{dW_c}{D_m}; N_b = \frac{\tau D_B(C_w - C_\infty)}{\vartheta};$$
$$N_t = \frac{\tau D_T(T_w - T_\infty)}{\vartheta T_\infty}; L_e = \frac{\alpha_f}{D_B}; R = \frac{4\sigma^* T_\infty^3}{k^* k}; \delta = \frac{Qx}{\rho c_p u_\infty};$$
$$E_c = \frac{(u_\infty)^2}{(c_p)_f(T_w - T_\infty)}; P_r = \frac{\vartheta}{\alpha_f}; A = \frac{(\mathrm{Re}_b)^{2/(n+1)}}{Re_a}; \mathrm{Re}_a = \frac{\rho x u_\infty}{a};$$
$$\mathrm{Re}_b = \frac{\rho x (u_\infty)^{(2-n)}}{b}$$

2.3 Coefficients of heat and mass transport

The main objective of this analysis is to determine the factors that engineers need to take into account when addressing heat and nanoparticle mass transfer. Defining these as follows: local Nusselt number $\mathrm{Nu}_x = \left(\frac{xq_w}{k(T_w - T_\infty)}\right)_{y=0}$ and local nanofluid Sherwood number $\mathrm{Sh}_x = \left(\frac{xq_w}{D_B(C_w - C_\infty)}\right)_{y=0}$, where $q_w = -k\left(\frac{\partial T}{\partial y}\right)_{y=0}$ is wall heat flux. Using the aforementioned transformations, these parameters will reduce to $(\mathrm{Re}_b)^{-1/(n+1)}\mathrm{Nu}_x = -\left(1 + \frac{4R}{3}\right)\theta'(0)$ and $(\mathrm{Re}_b)^{-1/(n+1)}\mathrm{Sh}_x = -\phi'(0)$.

3 Computational procedure

The examined physical problem is addressed by a system of partial differential equations that are reduced to a system of ordinary differential equations (ODEs) using appropriate similarity transformations. Furthermore, the converted system of nonlinear ODEs (12)–(17) is solved by using the bvp4c function. To achieve this, the system of ODEs (18)–(23) is converted to first-order ODEs, which can be summed up as follows:

Solution by bvp4c:

$f = y_1 ; f' = y_2 ; f'' = y_3 ; f' = y_3' ; \theta = y_4 ; \theta' = y_5 ; \theta'' = y_5' ; \phi = y_7 ; \phi' = y_7 ; \phi'' = y_7' ; \chi = y_8 ; \chi' = y_9 ; \chi'' = y_9'$

$$f''' = \frac{2y_2^2 + M^2y_2 - y_1y_3}{A + (-1)^{n-1}n(y_3)^{n-1}}, \tag{18}$$

$$\theta'' = y_5' = \frac{[P_ry_1y_5 + \delta P_ry_4 + P_rE_c(-y_3)^{(n+1)} + MP_rE_cy_2^2 + N_by_5y_7 + N_by_5^2 + AP_rE_c(y_3)^2]}{-\left(1 + \frac{4R}{3}\right)}, \tag{19}$$

$$y_7' = \phi'' = -\left[P_rL_ey_1y_7 + \frac{N_t}{N_b}y_5'\right] \tag{20}$$

$$y_9' = \chi'' = P_ey_7y_9 + P_ey_8\phi'' - L_by_1y_9. \tag{21}$$

Using boundary conditions

$$\text{at } \eta = 0 : y_0(1) = 0,\ y_0(2) - 1 = 0,\ y_0(4) - 1 = 0,\ y_0(6) - 1 = 0,\ y_0(8) - 1 = 0, \tag{22}$$

$$\text{for } \eta \to \infty : y_1(2) = 1,\ y_1,\ y_1(4) = 0,\ y_1(6) = 0,\ y_1(8) = 0. \tag{23}$$

The convenience with which nonlinear issues in simple domains can be dealt with is an advantage of this approach. The method is proven effective and precise in a number of boundary value problems and iteratively refined to a range of 10^{-5} and a step size of 0.05.

4 Results and discussion

In this section, we will focus on explaining the flow regime, or the conditions under which the nanofluid moves and behaves in terms of its velocity temperature, microorganism profile, and nanoparticle concentration. The scope of variables considered in this investigation is

$0 \le A \le 1.5,\ 0 \le M \le 1.5,\ 0 \le P_r \le 1.5,\ 0 \le E_c \le 1.5,\ 0 \le N_b \le 1.5,\ 0 \le N_t \le 1.5,\ 0 \le L_e \le 1.5,\ 0 \le R \le 1.5,\ 0 \le \delta \le 1.5,\ 0 \le L_b \le 1.5,\ 0 \le P_e \le 1.5.$

4.1 Effect of A on velocity, temperature, chemical reaction, motile density profiles

Figure 2(a) shows that the fluid velocity increases as Sisko fluid parameter (material parameter) increases. Due to the fact that the relationship between the material parameter and the fluid's viscosity is inverse. The observations from this study indicated that when the value of A was increased, the viscosity of the fluid decreased, leading to a subsequent reduction in the resistance encountered during fluid motion. The fluid velocity rises as a result. The effect of Sisko fluid parameter A (material parameter) on fluid temperature is shown in Figure 2(b). As the material parameter A is raised, a drop in the fluid temperature is seen.

4.2 Effect of M on velocity, temperature, nanoparticle concentration, and microorganism profiles

The purpose of Figure 3(a)–(d) is to explore how the velocity, temperature, volume proportion of nanoparticles, and

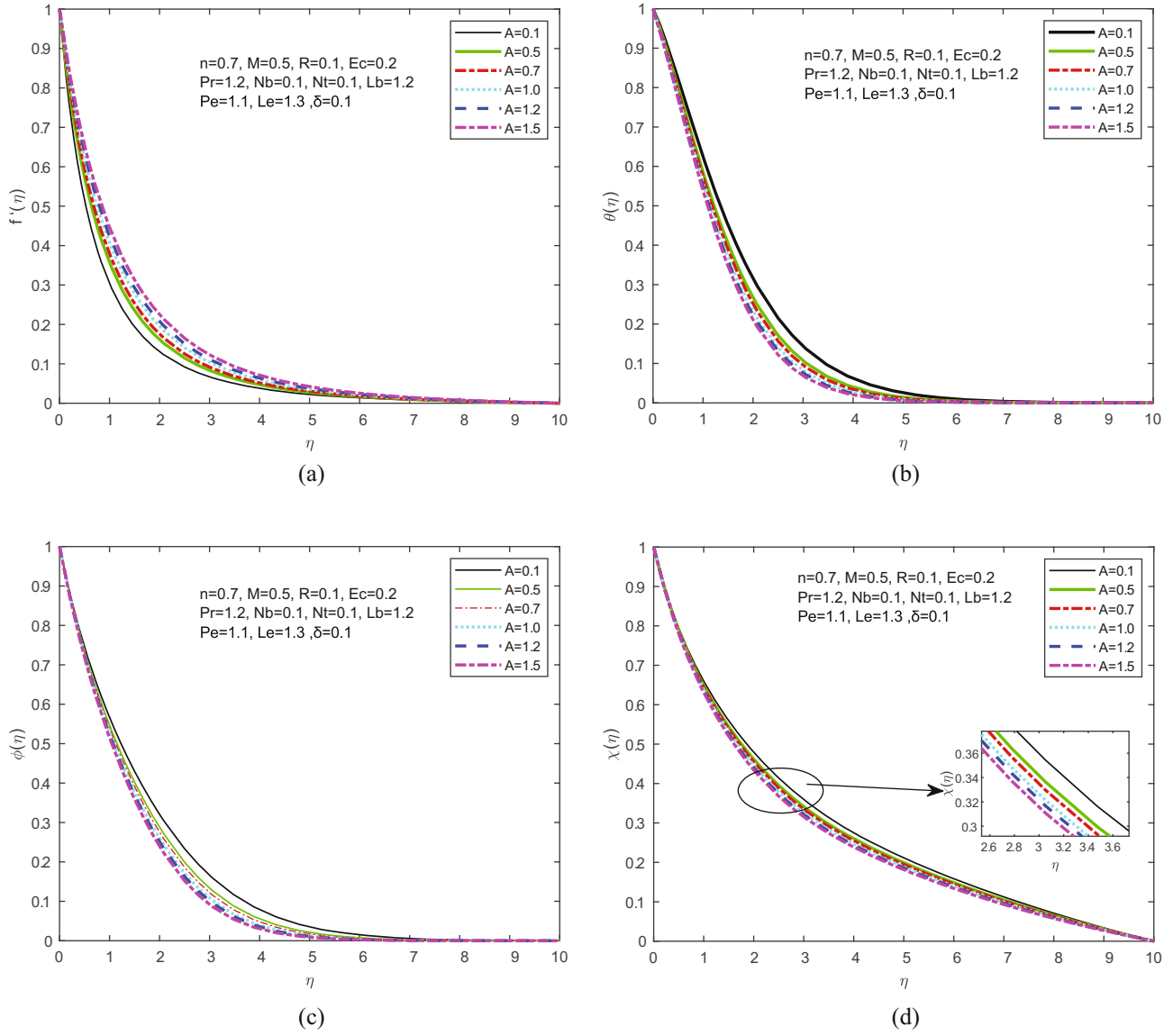

Figure 2: (a) f' *vs* A, (b) θ *vs* A, (c) ϕ *vs* A and (d) χ *vs* A.

microorganism density curves are influenced by the magnetic parameter (M). The velocity profile is observed to decrease as magnetic field strength estimates (M) increase, according to Figure 3(a), owing to the Lorentz force theorem, on which the magnetic field is established. The greater collisional impact between fluid atoms, as indicated by M, results in increased fluid flow resistance. Furthermore, the Lorentz force, which acts in opposition to the direction of flow, creates a resistance force that contributes to the thickness of the thermal boundary layer, as shown in Figure 3(b). The presence of a reversing force results in a decrease in the fluid flow, leading to a decline in the velocity field. Notably, Figure 3(c) and (d) demonstrate that the inclusion of magnetic parameters contributed to the enhancement of temperature and volume fraction near the surface, as well as the thicknesses of the thermal and nanoparticle concentration boundary layers. These outcomes can be explained by the increased heat generation associated with higher magnetic parameter values (M), which led to the expansion of temperature, concentration, and gyrotactic microorganism boundary layers, as depicted in Figure 3(b)–(d).

4.3 Effect of P_r on temperature, nanoparticle concentration profile, and microorganism profiles

The curves for the temperature, nanoparticle volume fraction, and density of the motile microorganisms are

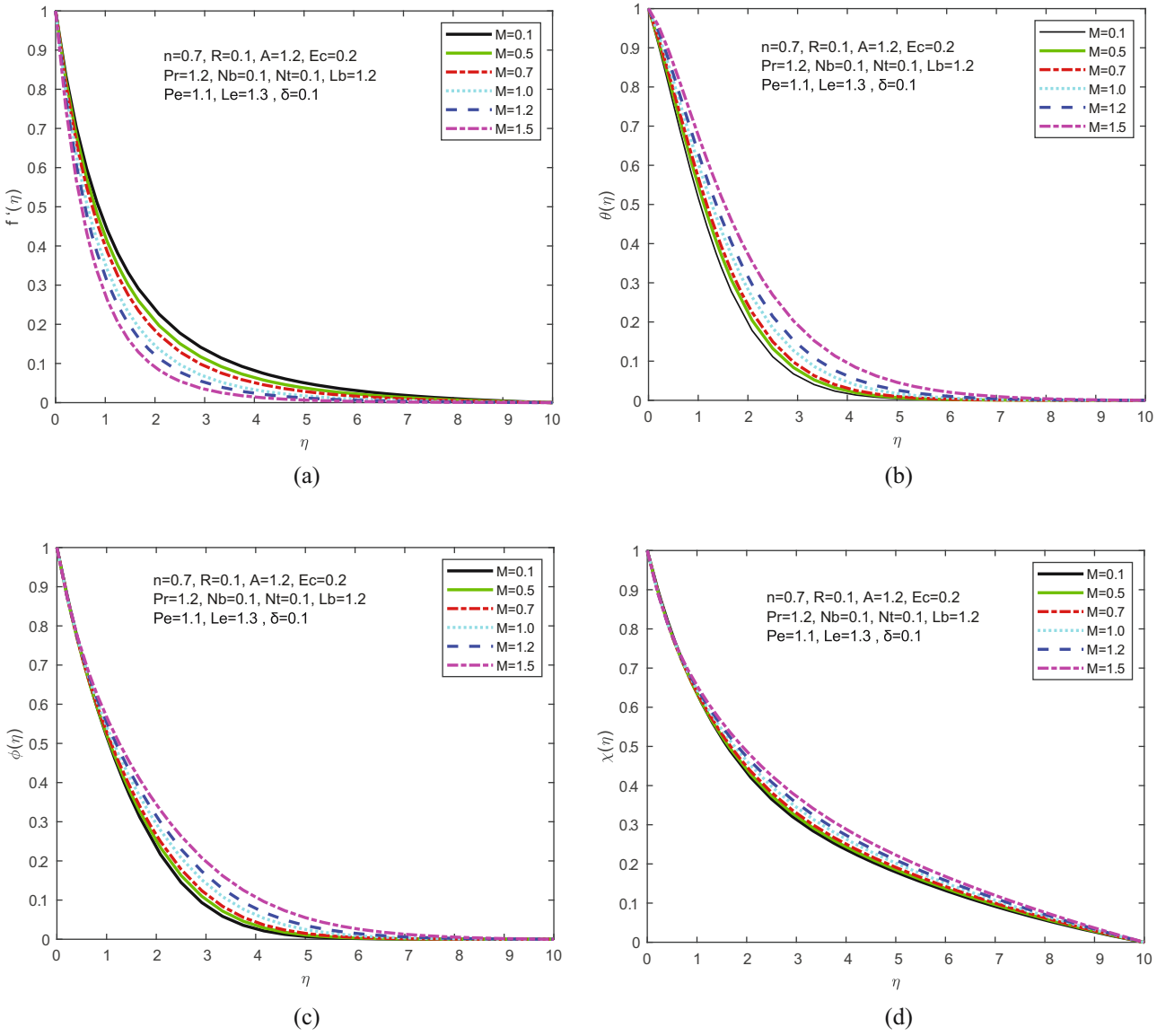

Figure 3: (a) f' *vs* M, (b) θ *vs* M, (c) ϕ *vs* M and χ *vs* M.

depicted in Figure 4(a)–(c), which illustrated the manner in which the Prandtl number P_r affected these curves. The Prandtl number had no effect on velocity, according to Eq. (9). As shown in Figure 4(a), the temperature and thickness of the thermal boundary layer decreased as P_r increased. In terms of physical significance, when P_r was raised, the thermal diffusivity dropped, leading to a reduction in the capability of energy to transfer across the thermal boundary layer. The thicknesses of the concentration boundary layer exhibited an upward trend as P_r increased as shown in Figure 4(b). The influence of the Prandtl number on the motile microorganism's density ($\chi(\eta)$) is shown in Figure 4(c), which indicates that the density of microorganisms increased with increasing P_r. This is due to the fact that the boundary layer thicknesses of the motile microorganisms decreased with increasing P_r, causing their size to decrease. In other terms, the increase in P_r resulted in a reduction in the number of gyrotactic microbes.

4.4 Effect of E_c on temperature, nanoparticle concentration profile, and microorganism profiles

In Figure 5(a)–(c), temperature, concentration, and microorganism density variations are depicted for different

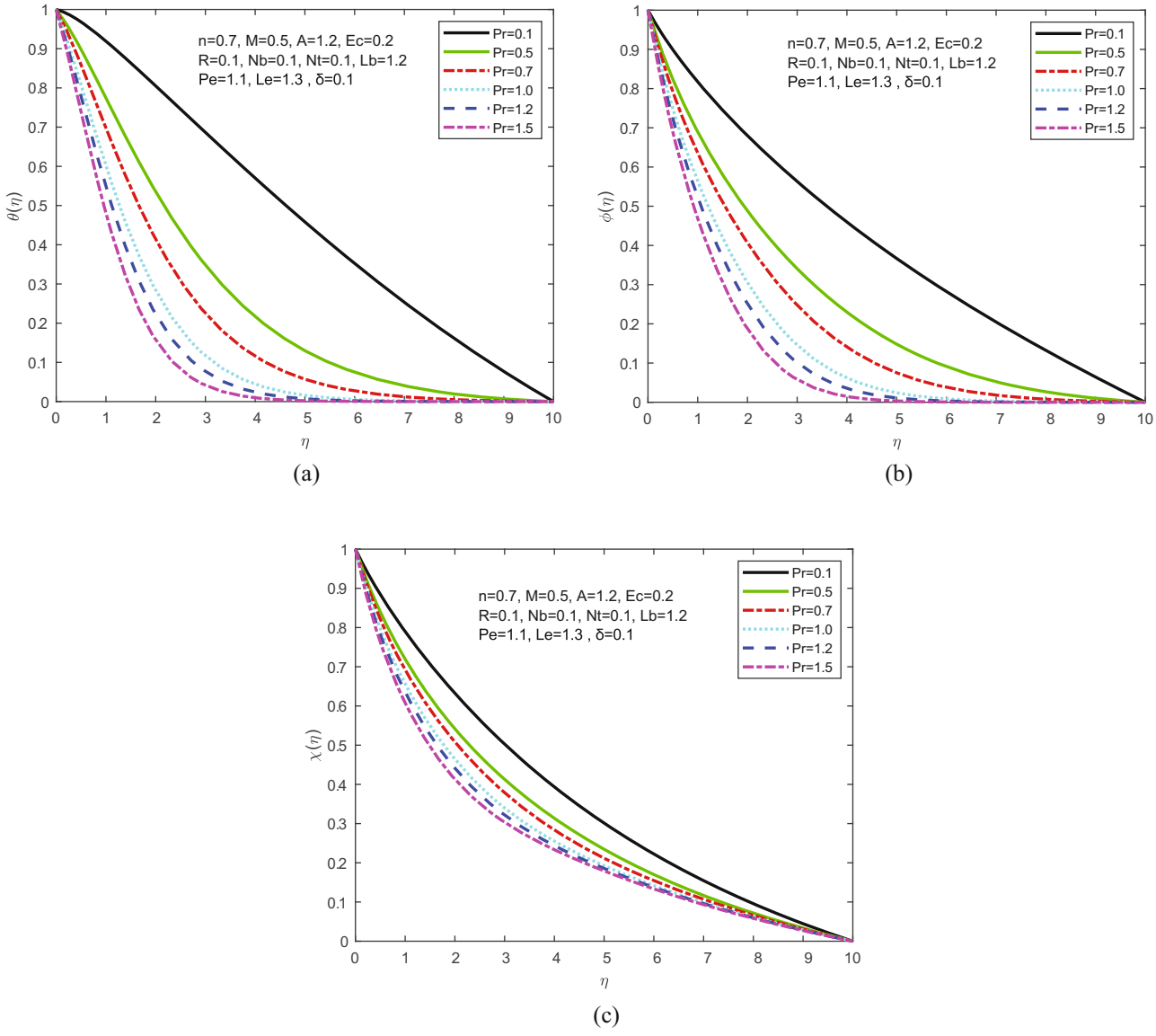

Figure 4: (a) θ *vs* P_r, (b) ϕ *vs* P_r, and (c) χ *vs* P_r.

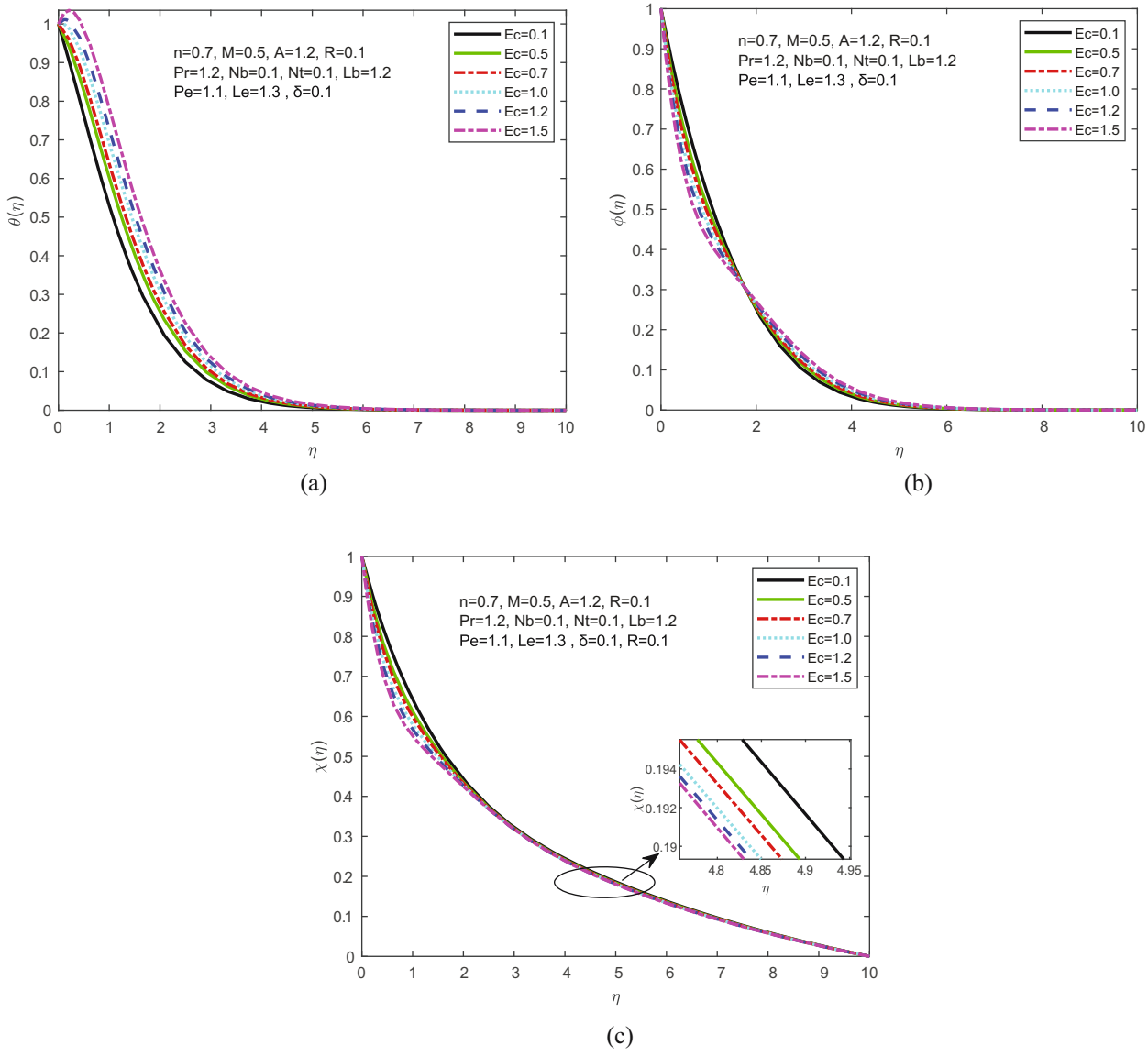

Figure 5: (a) θ *vs* E_c, (b) ϕ *vs* E_c and (c) χ *vs* E_c.

Eckert number (E_c) values. These figures illustrate that an elevated Eckert number leads to an increase in fluid temperature. This effect arises from the fact that E_c represents the ratio between kinetic energy and enthalpy, and as E_c increases, so does kinetic energy. Consequently, fluid particles collide more frequently, converting kinetic energy into thermal energy and resulting in higher fluid temperatures. It was observed that when E_c increased, the density of microorganism dropped. When the Eckert number increases in the fluid flow, it implies that there is a higher rate of heat transfer. Elevated temperatures resulting from increased heat transfer can be detrimental to microorganisms, leading to a drop in their density due to thermal stress.

4.5 Effect of N_b on temperature, nanoparticle concentration profile, and microorganism profiles

Figure 6(a) and (b) depict the impact of the N_b on the temperature and nanoparticle volume fraction trajectories. The temperature boundary layer was shown to be improved as N_b increased; however, the nanoparticle volume fraction boundary thickness had the reverse effect. Based on the information presented in Figure 6(b), it is evident that the Brownian motion parameter contributes to a decrease in the thickness of the concentration boundary layer, leading to a subsequent decline in the concentration. The particles travel

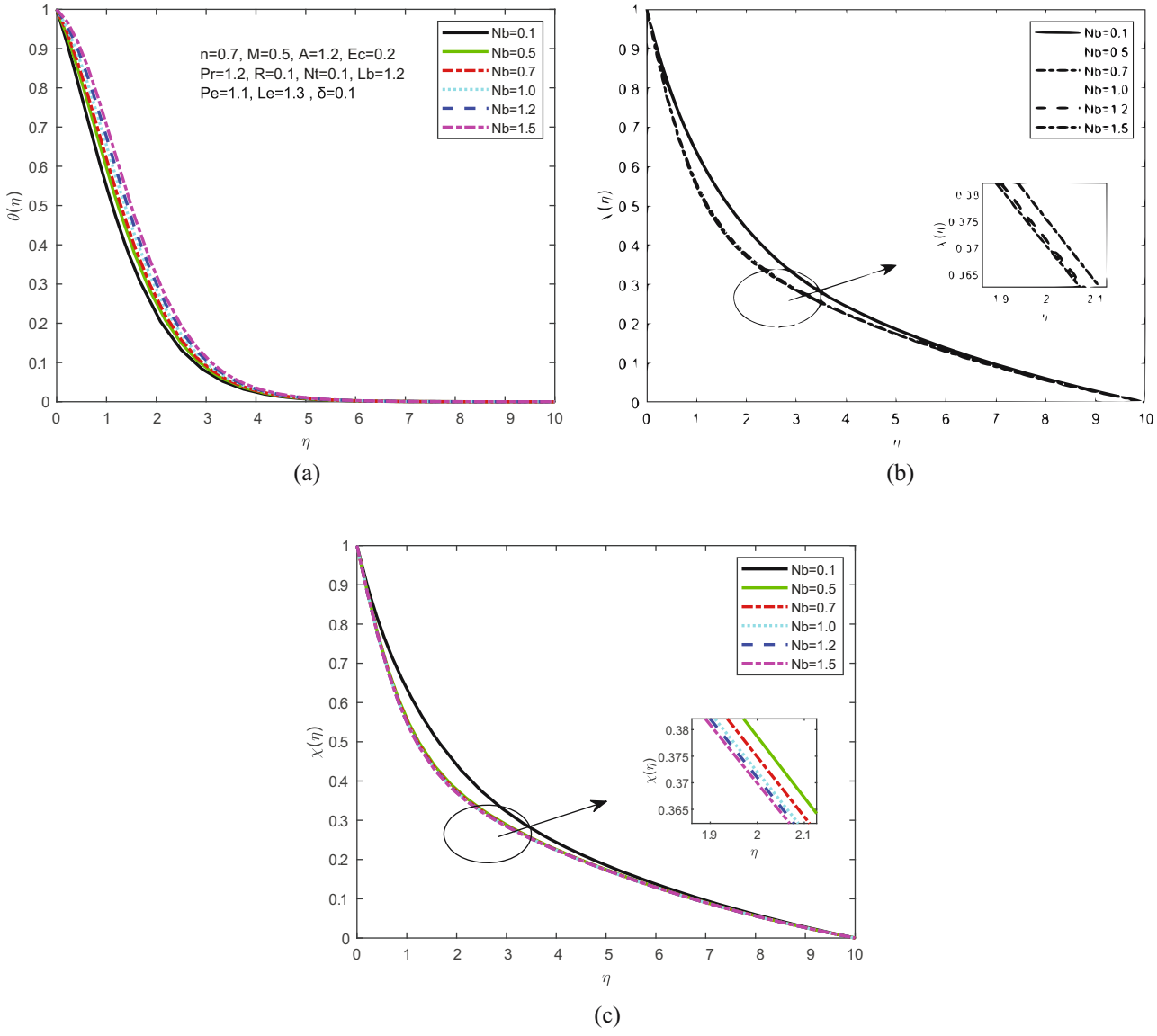

Figure 6: (a) θ *vs* N_b, (b) ϕ *vs* N_b and (c) χ *vs* N_b.

arbitrarily as a result of the greater Brownian motion, which is another physical explanation for the situation. This random movement results in additional heat being emitted. Hence, the formation of temperature curves was investigated. In addition, N_b has no effect on the motile microbe profiles' density and velocity.

4.6 Effect of δ on temperature, nanoparticle concentration profile, and microorganism profiles

Furthermore, the heat sink parameter (δ) represents the rate of heat removal or dissipation from a system. A higher δ signifies more efficient cooling, leading to a lower temperature (Figure 7(a)). As shown in Figure 7(b), a higher δ indicates more efficient cooling and enhanced fluid motion, resulting in better nanoparticle dispersion and reduced concentration. An increase in the heat sink parameter (δ) leads to an increase in microorganism density profiles due to improved thermal regulation (Figure 7(c)).

4.7 Effect of L_e on nanoparticle concentration profile and microorganism profiles

By analysing Figure 8(a) and (b), it was evident that an elevated value of L_e led to a decline in concentration

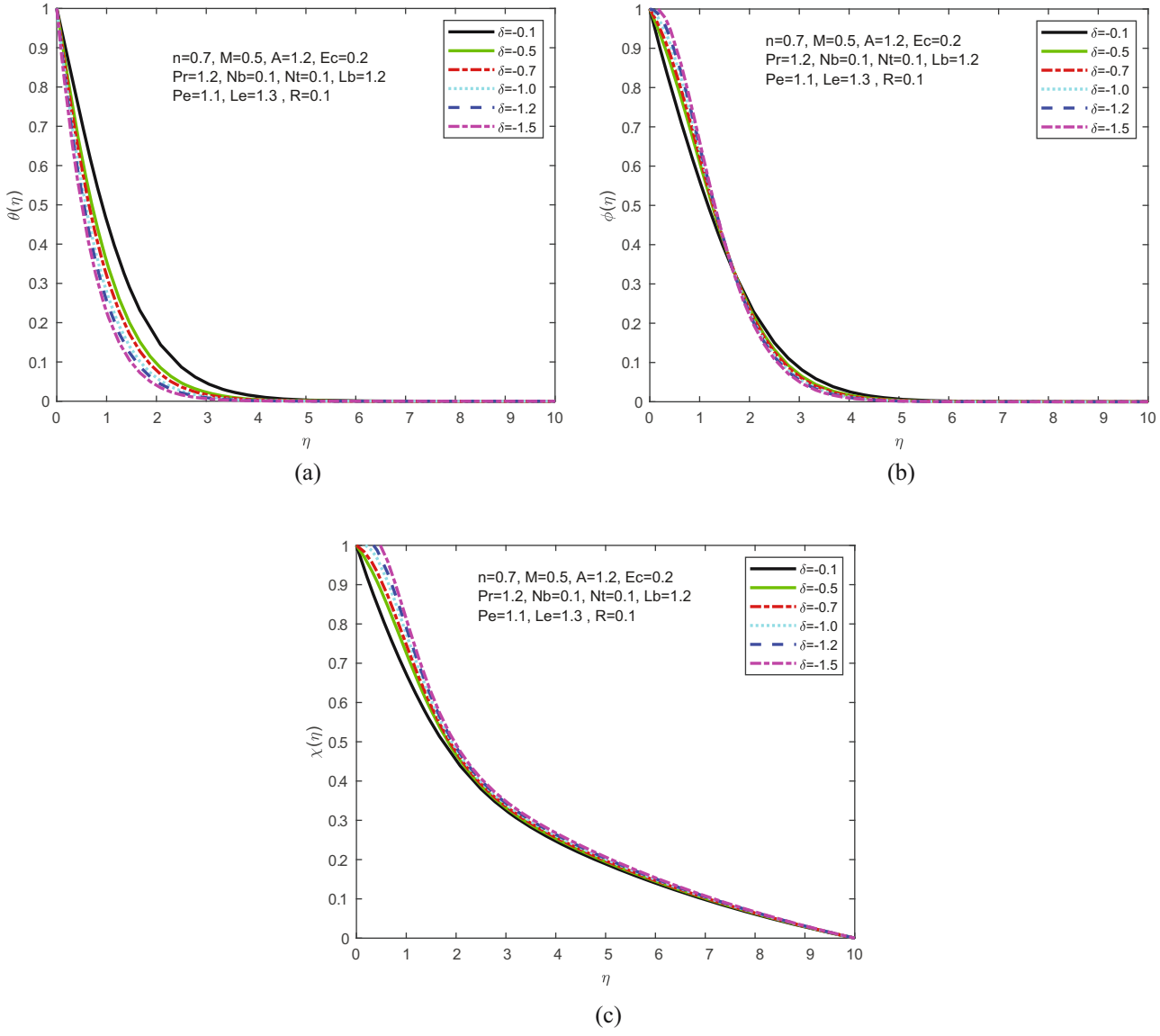

Figure 7: (a) θ *vs* δ, (b) ϕ *vs* δ, and (c) χ *vs* δ.

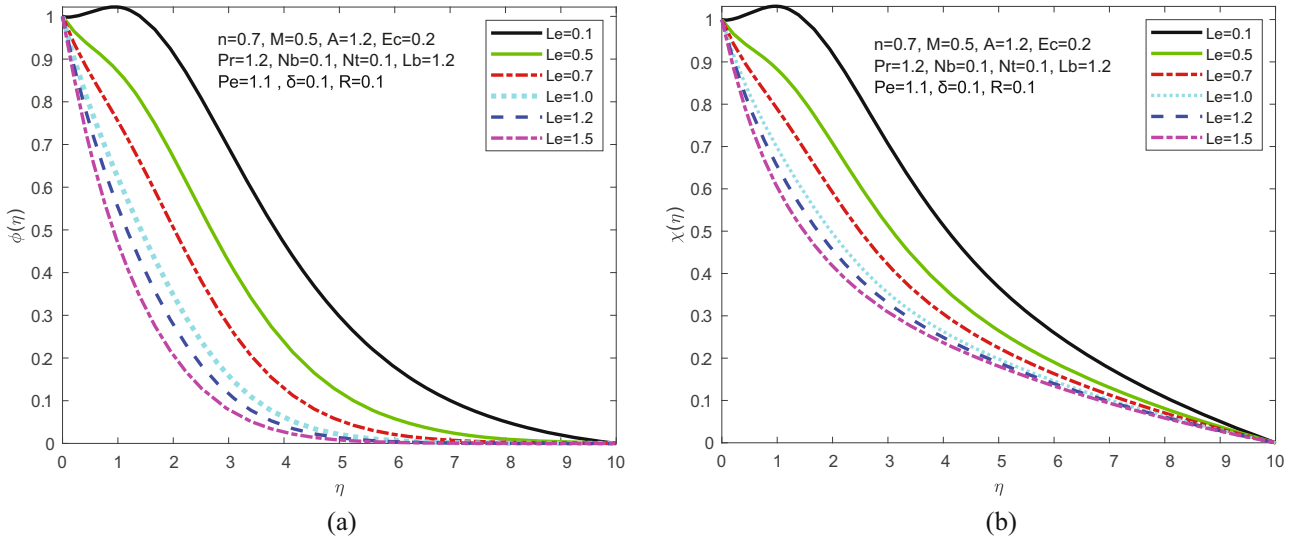

Figure 8: (a) ϕ *vs* L_e and (b) χ *vs* L_e.

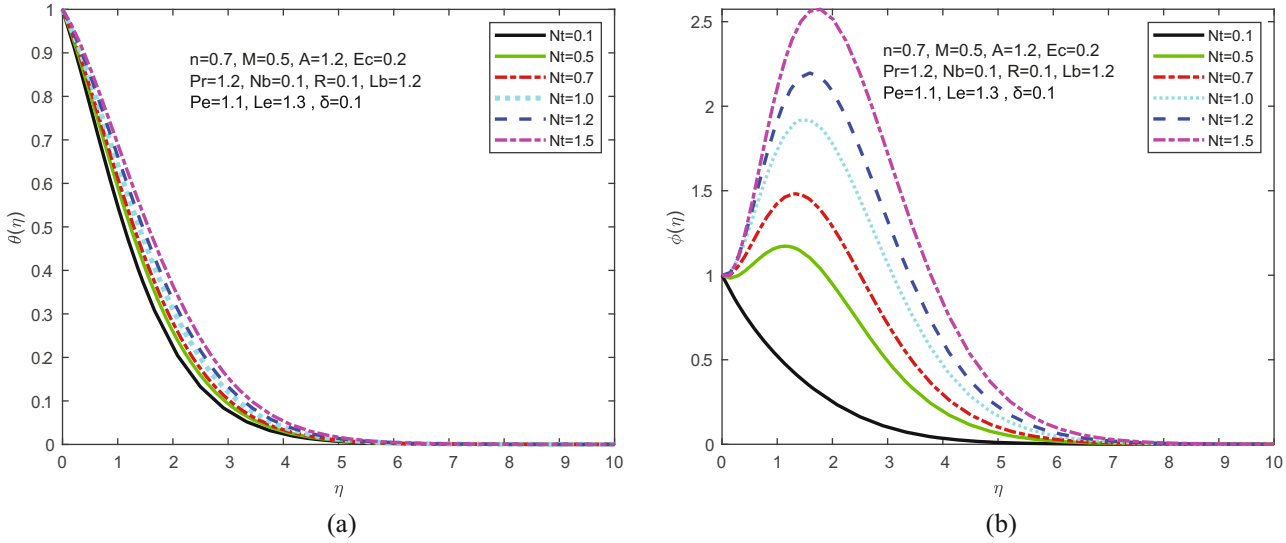

Figure 9: (a) θ *vs* N_t and (b) ϕ *vs* N_t.

profile, and on the other hand, the trend was reversed for the microorganism profile at $\eta \approx 1.2$. In the region where $\eta < 1.2$, the increase in L_e resulted in a decrease in the thickness of the microorganism boundary layers. while, for $\eta > 1.2$, the reverse trend was observed with increasing L_e. The effect of L_e on concentration is further illustrated in Figure 8(a), where it was observed that concentration decreased as L_e increased. The underlying explanation is that as L_e increases, mass diffusivity decreases, resulting in a reduction in the depth of penetration of the boundary layer.

4.8 Effect of N_t on temperature, nanoparticle concentration profile, and microorganism profiles

Variations in the thermophoresis parameter N_t are reflected in Figure 9(a) and (b), illustrating the impact on the temperature and nanoparticle fraction curves. The results demonstrate that N_t has a significant impact on both temperature and nanoparticle fraction. This phenomenon occurs due to the increase in the thermal boundary layer density caused by the thermophoresis parameter. As observed in Figure 9(a), an increase in N_t results in an increase in temperature. The microscopic fluid particles involved in thermophoresis activities are drawn from the warm to the cold region, resulting in an improvement in temperature, thermal boundary layer, and nanoparticle volume fraction profiles. However, N_t has no impact on velocity and density curves of motile microorganism.

The local Nusselt number $[-\theta'(0)]$ for different parameters is compared with the results obtained by [15,33–35] in Table 1. It demonstrates excellent agreement between

Table 1: Comparison of local Nusselt number $-\theta'(0)$ for different values of P_r for $L_e = P_e = E_c = N_t = L_b = N_b = M = 0$

P_r	Ref. [15]	Ref. [33]	Ref. [34]	Ref. [35]	Current study
1	0.954782	0.954782	0.9547	0.954955	0.954779
1.5	1.234755				1.234823
2	1.471460		1.4714		1.471454
2.5	1.680229				1.680225
3	1.869073	1.869075	1.8691	1.869074	1.869072
5	2.500131	2.50013		2.500184	2.500139

Table 2: Comparison of Sherwood number $[-\phi'(0)]$ for different values of N_b, N_t, and P_r taking $L_e = P_e = E_c = L_b = 0$

N_b	N_t	P_r	Sh_x $n = 0$		Sh_x $n = 1$	
			Jawad *et al.* [36]	Current Study	Jawad *et al.* [36]	Current Study
0.1	0.5	1.5	−1.35820	−1.3479	−1.35938	−1.35859
0.5			−0.238811	−0.23792	−0.239002	−0.238092
1.0			−0.098888	−0.98742	−0.098954	−0.098879
1.5	0.1		0.0223188	0.022217	0.0223610	0.02228
	0.5		−1.35820	−1.35789	−1.35938	−1.35876
	1.0		−2.75366	−2.75306	−2.75610	−2.75532
	1.5		−4.14542	−4.14483	−4.14910	−4.14725
		3.0	−1.21912	−1.21754	−2.06224	−2.06212
		5.0	−1.53875	−1.53779	−2.45134	−2.45124

the current study and those obtained in the aforementioned studies.

Table 2 depicts the influence of Sherwood number due to various parameters. It is noticed that an elevation in the thermophoresis parameter causes an upward trend in local Sherwood number values, whereas an elevation in the Prandtl number results in a reduction in the Sherwood number.

5 Conclusions

In the current framework, this study investigates the MHD fluid flow of a dissipative Sisko nanofluid containing microorganisms moving along an exponentially stretched sheet. Using the bvp4c solver, numerical results for the converted mathematical model are calculated. The significant results are enumerated as follows:

1) Because of the inverse relationship between the material parameter (A) and the viscosity of the fluid. Observations from this study revealed that as the value of A increased, the fluid's viscosity decreased, resulting in a reduction in the resistance encountered during fluid motion. As a consequence, the fluid velocity increases.
2) Both temperature and nanoparticle fraction are significantly affected by the thermophoresis parameter (N_t). This phenomenon occurs because the increase in N_t increases the thermal boundary layer density.
3) When the Eckert number of a fluid increases, it indicates a higher rate of heat transfer. Microorganisms may experience a decrease in density as a consequence of thermal stress when exposed to elevated temperatures caused by increased heat transfer.
4) The increase in Prandtl number (P_r) resulted in a decrease in thermal diffusivity, hence causing a decline in the efficiency of energy transmission across the thermal boundary layer. The thickness of the concentration boundary layer demonstrated an increasing trend as the P_r grew.

Acknowledgments: The authors extend their appreciation to the Deanship of Scientific Research at King Khalid University (KKU) for funding this research through the Research Group Program under the grant number (R.G.P.2/453/44).

Funding information: This research is funded by the Deanship of Scientific Research at King Khalid University (KKU) for funding this research through the Research Group Program under the grant number (R.G.P.2/453/44).

Author contributions: All authors have accepted responsibility for the entire content of this manuscript and approved its submission.

Conflict of interest: The authors state no conflict of interest.

Data availability statement: All data generated or analysed during this study are included in this published article.

References

[1] Shahid A, Huang H, Bhatti MM, Zhang L, Ellahi R. Numerical investigation on the swimming of gyrotactic microorganisms in nanofluids through porous medium over a stretched surface. Mathematics. 2020;8(3):380.
[2] Choi SUS, Singer DA, Wang HP. Developments and applications of non-Newtonian flows. ASME Fed. 1995;66:99–105.
[3] Buongiorno J. Convective transport in nanofluids. J Heat Transf. 2006;128:240–50.
[4] Eastman JA, Choi US, Li S, Thompson LJ, Lee S. Enhanced thermal conductivity through the development of nanofluids. MRS Proc. 1996;457:3–11.
[5] Sheikholeslami M, Ganji DD, Javed MY, Ellahi R. Effect of thermal radiation on magnetohydrodynamics nanofluid flow and heat transfer by means of two-phase model. J Magn Magn Mater. 2015;374:36–43.
[6] Pourfattah F, Arani AAA, Babaie MR, Nguyen HM, Asadi A. On the thermal characteristics of a manifold microchannel heat sink subjected to nanofluid using two-phase flow simulation. Int J Heat Mass Transf. 2019;143:118518.
[7] Asadi A, Aberoumand S, Moradikazerouni A, Pourfattah F, Żyła G, Estellé P, et al. Recent advances in preparation methods and thermophysical properties of oil-based nanofluids: A state-of-the-art review. Powder Technol. 2019;352:209–26.
[8] Khan M, Shahid A, Malik MY, Salahuddin T. Thermal and concentration diffusion in Jeffery nanofluid flow over an inclined stretching sheet: A generalized Fourier's and Fick's perspective. J Mol Liq. 2018;251:7–14.
[9] Asadi A, Alarifi IM, Ali V, Nguyen HM. An experimental investigation on the effects of ultrasonication time on stability and thermal conductivity of MWCNT-water nanofluid: Finding the optimum ultrasonication time. Ultrason Sonochem. 2019;58:104639.
[10] Zeeshan A, Riaz A, Alzahrani F, Moqeet A. Flow analysis of two-layer Nano/Johnson–Segalman fluid in a blood vessel-like tube with complex peristaltic wave. Math Probl Eng. 2022;2022:Article ID 5289401, 18.
[11] Riaz A, Khan SU, Zeeshan A, Khan SU, Hassan M, Muhammad T. Thermal analysis of peristaltic flow of nanosized particles within a curved channel with second-order partial slip and porous medium. J Therm Anal Calorim. 2021;143:1997–2009.
[12] Riaz A, Ellahi R, Sait SM, Muhammad T. Magnetized Jeffrey nanofluid with energy loss in between an annular part of two micro non-concentric pipes. Energy Sources Part A: Recovery Util Environ Eff. 2022;44(3):8314–33.
[13] Tlili I, Nabwey HA, Ashwinkumar GP, Sandeep N. 3-D magnetohydrodynamic AA7072-AA7075/methanol hybrid nanofluid flow above an uneven thickness surface with slip effect. Sci Rep. 2020;10:1–13.

[14] Chamkha AJ, Rashad AM, Alsabery AI, Abdelrahman ZMA, Nabwey HA. Impact of partial slip-on magneto-ferrofluids mixed convection flow in enclosure. J Therm Sci Eng Appl. 2020;12:051002.
[15] Ferdows M, Nabwey HA, Rashad AM, Uddin MJ, Alzahrani F. Boundary layer flow of a nanofluid past a horizontal flat plate in a Darcy porous medium: A Lie group approach. Proceedings of the Institution of Mechanical Engineers, Part C: Journal of Mechanical Engineering Science; 2019.
[16] Kuznetsov AV. Bio-thermal convection induced by two different species of microorganisms. Int Commun Heat Mass Transf. 2011;38:548–53.
[17] Alloui Z, Nguyen TH, Bilgen E. Bioconvection of gravitactic micro-organisms in a vertical cylinder. Int Commun Heat Mass Transf. 2005;32:739–47.
[18] Waqas H, Hussain M, Alqarnib MS, Eid MR, Muhammad T. Numerical simulation for magnetic dipole in bioconvection flow of Jeffrey nanofluid with swimming motile microorganisms. Waves Random Complex Media. 2021;3:1–18.
[19] Waqas H, Imran M, Muhammad T, Salt SM, Ellahi R. Numerical investigation on bioconvection flow of Oldroyd-B nanofluid with non-linear thermal radiation and motile microorganisms over rotating disk. J Therm Anal Calor. 2021;145:523–39.
[20] Uddin MJ, Kabir MN, Bég OA. Computational investigation of Stefan blowing and multiple-slip effects on buoyancy-driven bioconvection nanofluid flow with microorganisms. Int J Heat Mass Transf. 2016;95:116–30.
[21] Chamkha AJ, Rashad AM, Kameswaran PK, Abdou MMM. Radiation effects on natural bioconvection flow of a nanofluid containing gyrotactic microorganisms past a vertical plate with streamwise temperature variation. J Nanofluids. 2017;6:587–95.
[22] Rashad AM, Nabwey HA. Gyrotactic mixed bioconvection flow of a nanofluid past a circular cylinder with convective boundary condition. J Taiwan Inst Chem Eng. 2019;99:9–17.
[23] Alwatban AM, Khan SU, Waqas H, Tlili I. Interaction of Wu's slip features in bioconvection of Eyring Powell nanoparticles with activation energy. Process. 2019;7:859.
[24] Aziz A, Khan WA, Pop I. Free convection boundary layer flow past a horizontal flat plate embedded in porous medium filled by nanofluid containing gyrotactic microorganisms. Int J Therm Sci. 2012;56:48.
[25] Shaw S, Sandile Motsa S, Sibanda P. Magnetic field and viscous dissipation effect on bioconvection in a permeable sphere embedded in a porous medium with a nanofluid containing gyrotactic micro-organisms. Heat Transf – Asian Res. 2018;47:718–34.
[26] Rashad AM, Chamkha A, Mallikarjuna B, Abdou MMM. Mixed bioconvection flow of a nanofluid containing gyrotactic microorganisms past a vertical slender cylinder. Front Heat Mass Transf. 2018;10. http://dx.doi.org/10.5098/hmt.10.21.
[27] Elboughdiri N, Reddy CS, Alshehri A, Eldin SM, Muhammad T, Wakif A. A passive control approach for simulating thermally enhanced Jeffery nanofluid flows nearby a sucked impermeable surface subjected to buoyancy and Lorentz forces. Case Stud Therm Eng. July 2023;47:103106.
[28] Sharma J, Ahammad NA, Wakif A, Shah NA, Chung JD, Weera W. Solutal effects on thermal sensitivity of casson nanofluids with comparative investigations on Newtonian (water) and non-Newtonian (blood) base liquids. Alex Eng J. May 2023;71:387–400.
[29] Wakif A. Numerical inspection of two-dimensional MHD mixed bioconvective flows of radiating Maxwell nanofluids nearby a convectively heated vertical surface. Waves Random Complex Media. 2023;1–22. doi: 10.1080/17455030.2023.2179853.
[30] Puneeth V, Sarpabhushana M, Anwar MS, Aly EH, Gireesha BJ. Impact of bioconvection on the free stream flow of a pseudoplastic nanofluid past a rotating cone. Heat Transf. 2022;51(5):4544–61.
[31] Jan A, Mushtaq M, Farooq U, Hussain M. Nonsimilar analysis of magnetized Sisko nanofluid flow subjected to heat generation/absorption and viscous dissipation. J Magnetism Magnetic Mater. 2022;564(2):170153.
[32] Ferdows M, Zaimi K, Rashad AM, Nabwey HA. MHD bioconvection flow and heat transfer of nanofluid through an exponentially stretchable sheet. Symmetry. 2020;12:692.
[33] Magyari E, Keller B. Heat and mass transfer in the boundary layers on an exponentially stretching continuous surface. J Phys D Appl Phys. 1999;32:577–85.
[34] Biliana B, Nazar R. Numerical solution of the boundary layer flow over an exponentially stretching sheet with thermal radiation. Eur J Sci Res. 2009;33:710–7.
[35] Loganthan P, Vimala C. MHD flow of nanofluids over an exponentially stretching sheet embedded in a stratified medium with suction and radiation effects. J Appl Fluid Mech. 2015;8:85–93.
[36] Jawad M, Shah Z, Islam S, Khan W, Khan AZ. Nanofluid thin film flow of Sisko fluid and variable heat transfer over an unsteady stretching surface with external magnetic field. J Algorithms Comput Technol. 2019;1748301819832456.